Sensors and Materials, Vol. 38, No. 4 (2026) 1769–1786
MYU Tokyo

S & M 4405

Graphene Transistor Modified with Phenylboronic Acid Carbon Quantum Dots for Specific Recognition of Sugar Molecules with Cis-diol Structure

JiaHui Li,[1] Wei Qin,[1] and ChunRui Chang[2*]

[1]School of Electrical Engineering, North China University of Science and Technology,
No. 21 Bohai Road, Caofeidian District, Tangshan, Hebei 063210, China
[2]School of Science,North China University of Science and Technology,
No. 21 Bohai Road, Caofeidian District, Tangshan, Hebei 063210, China

(Received November 14, 2025; accepted February 16, 2026)

Keywords: graphene, field-effect transistor, carbon quantum dots, cis-diol structure, sugar molecules

Considering the reversible formation of cyclic boronic esters between boronic acid groups and cis-diol structures, in this study, we develop a graphene field-effect transistor (GFET) device functionalized with phenylboronic acid carbon quantum dots for the sensitive and real-time detection of sugars containing cis-diol structures. The results demonstrate that the device achieves a minimum detection limit of 10 fM for glucose and sialic acid, and exhibits excellent linear relationships between channel current changes and logarithmic concentrations in the range of 10 fM–0.1 mM, with linear fitting coefficients greater than 0.97. Notably, glucose shows a higher absolute current response, while sialic acid exhibits a larger current change sensitivity, indicating the potential advantage of the device in detecting complex biomolecules. In contrast, the detection results for sucrose molecules without the cis-diol structure, long-chain starch with a spatial structure, and common serum interferents such as ascorbic acid, Na^+, and K^+ further show that the device has good selectivity for molecules containing the cis-diol structure and is affected by molecular steric hindrance and molecular stability. Combining the biological functions of glucose and sialic acid, along with the advantages of miniaturization, integration, and rapid response, the developed sensor platform holds promise for flexible, miniaturized applications, providing a practical tool for the real-time monitoring and early diagnosis of tumor biomarkers.

1. Introduction

Cancer is one of the leading causes of death worldwide, with one in four deaths attributed to cancer, making it the leading cause of mortality among all diseases.(1) Tumor biomarkers (TBMs) refer to substances synthesized or secreted by tumor cells, or produced by the body in response to tumor cells, during the occurrence and development of malignancies.(2,3) The detection of tumor biomarkers plays a critical role in disease monitoring, treatment guidance, and prognosis

*Corresponding author: e-mail: changchunrui@ncst.edu.cn
https://doi.org/10.18494/SAM6027

ISSN 0914-4935
https://myukk.org/

evaluation, which can effectively compensate for the shortcomings of other medical technologies in tumer diagnosis, treatment, and prognosis judgment. In the tumor microenvironment, sialic acid, as a terminal-modified sialylated sugar chain, is widely distributed in various glycoproteins and glycolipids. Its levels are significantly elevated in several malignant tumors, including liver cancer, lung cancer, and breast cancer, making it an important potential tumor biomarker.[4,5] Moreover, glucose, as the primary energy source for cells, exhibits abnormal uptake and metabolism in tumor cells, particularly under the "aerobic glycolysis" effect (i.e., the Warburg effect), where glucose uptake is enhanced and can serve as a valuable auxiliary biomarker for reflecting the metabolic state of tumors.[6,7]

In recent years, liquid-gated graphene field-effect transistor (LG-GFET)-based biosensing platforms have shown significant advantages in the field of tumor biomarker detection.[8–11] Kou *et al.*[12] developed a biosensor based on polyethylene glycol-modified graphene FETs, which effectively suppressed nonspecific adsorption in physiological media by optimizing the length of polyethylene glycol. This enabled the ultrasensitive and specific detection of cervical-cancer-related cytokines in undiluted, high-ion-strength physiological media, providing an important method for the immediate diagnosis of the disease. On the other hand, de Oliveira *et al.*[13] successfully developed an LG-GFET sensor suitable for wearable health monitoring, which utilized reduced graphene oxide to rapidly and selectively detect K^+ and Na^+ in artificial sweat environments, providing a promising solution for next-generation wearable monitoring technologies based on sweat analysis.

Researchers have shown that the LG-GFETs functionalized with phenylboronic acid carbon quantum dots can use graphene as the transistor channel. Because of the excellent electrical properties of graphene,[14–16] as well as the ability of phenylboronic acid and its derivatives to form reversible covalent bonds with cis-diol structures, the sensor is endowed with specific recognition capabilities for sugar molecules. Sialic acid and glucose, as typical sugar molecules containing cis-diol structures, can form reversible boronic-acid–diol coordination bonds with the phenylboronic acid group, leading to changes in charge transfer behavior. This mechanism makes them important recognition targets in FET sensors.[17,18]

In this study, a highly sensitive, highly selective, and real-time-detection phenylboronic acid carbon quantum dot–functionalized LG-GFET sensor was developed by modifying the gate with phenylboronic acid carbon quantum dots. This sensor was designed for the specific recognition of tumor-related biomarkers, such as sialic acid and glucose with cis-diol structures, thereby providing an electrochemical sensing platform that simultaneously exhibits tumor biomarker specific recognition and multitarget response capabilities. To validate the performance of the device, the regulation of sensor transfer characteristics and source–drain current responses to different concentrations of sialic acid and glucose was systematically investigated. Then, the correlation between electrical signals and target molecule concentrations was analyzed, providing strong technical support for early cancer screening.

2. Experimental Section

2.1 Reagents and instruments

The reagents used include acetone (≥99.5%), anhydrous ethanol (≥99.7%) (China National Pharmaceutical Group Chemical Reagents Co., Ltd.); phosphate-buffered saline (PBS, 10×, pH~7.4), mercaptoacetic acid ($HS-CH_2-COOH$), 1-(3-dimethylaminopropyl)-3-ethylcarbodiimide hydrochloride (EDC), N-hydroxysuccinimide (NHS), methacrylic acid (MAA), sodium lignosulfonate, 3-aminophenylboronic acid, glucose, sucrose, starch, and sialic acid (98%, Shanghai Aladdin Biochemical Technology Co., Ltd.); monolayer graphene (Hefei Microcrystal Materials Technology Co., Ltd.); and polymethyl methacrylate (PMMA, Sigma-Aldrich Biochemical Technology Co., Ltd.). All reagents are of analytical grade, and ultrapure water is used in experiments. The structural formulas of glucose, sucrose, sialic acid, and starch are shown in Fig. 1.

The instruments used include the testing platform (North China University of Science and Technology); H-765 transmission electron microscope (Hitachi, Japan); BX63F fluorescence microscope (Olympus, Japan); TH1992 digital source meter (Changzhou Tonghui Electronic Co., Ltd.); K575XD magnetron sputtering system (Shanghai MicroNano International Trading Co., Ltd.); Beckman Coulter Allegra X-15R centrifuge (Beckman Coulter, USA); hot air drying oven (Shanghai Yiheng Scientific Instruments Co., Ltd.); ultrasonic cleaner (Kunshan Ultrasonic Instrument Co., Ltd.); magnetic heating stirrer (Thermo Fisher Scientific); and 50 ml reaction kettle.

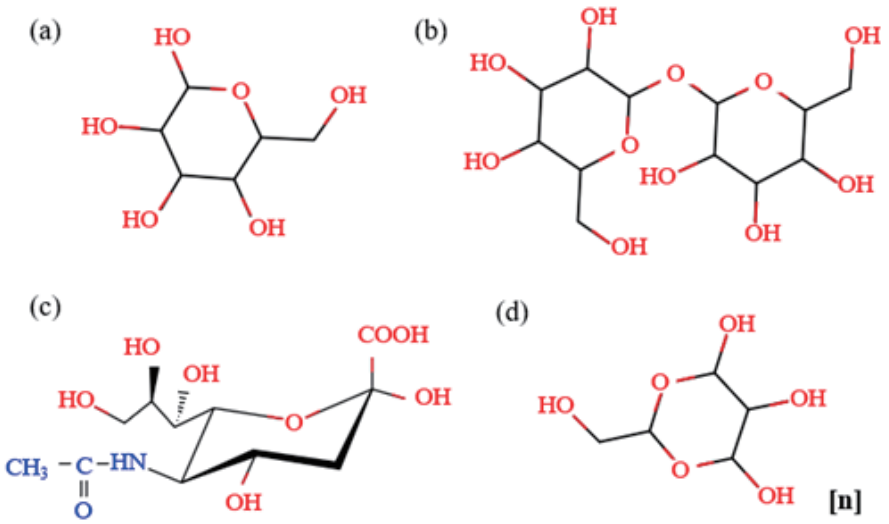

Fig. 1. (Color online) Molecular structures of carbohydrates: (a) glucose; (b) sucrose; (c) sialic acid; (d) starch.

2.2 Sample preparation and transistor fabrication

2.2.1 Preparation of carbon quantum dot stock solution

Dissolve 50 mg of 3-aminophenylboronic acid and 10 mg of sodium lignosulfonate in 10 mL of anhydrous ethanol, mix, and then transfer the mixture into the PTFE liner of a 50 mL reaction vessel. Heat the reaction mixture to 200 ℃ and let it react for 9 h. After the reaction, allow the product to cool to room temperature, then centrifuge at 12000 rpm for 10 min. Collect the upper clear liquid and filter it through a 0.22 μm filter membrane. Transfer the filtrate into a 1000 Da dialysis bag and dialyze in deionized water for about 72 h. Finally, remove the dialysis solution and concentrate it at 80 ℃ to obtain the phenylboronic acid carbon quantum dot stock solution.

2.2.2 Design and fabrication of graphene transistors

In the experiment, single-crystal silicon was selected as the substrate material. A planar transistor device with dimensions of 16 × 20 mm^2 was designed, as shown in Fig. 2(a). The source (S), drain (D), and gate (G) are coplanar, with the source–drain channel designed as a narrow, elongated structure measuring 10 mm in width and 0.2 mm in length. The gate is designed as a square modification electrode with dimensions of 3 × 3 mm^2.

In accordance with the designed transistor structure, chromium (20 nm thick) and gold (200 nm thick) were first deposited onto the substrate as electrodes using a magnetron sputtering system. The substrate was then cleaned by ultrasonic cleaning with ethanol and deionized water. Next, a 6 × 8 mm monolayer suspended graphene sheet was transferred to the channel region between the source and the drain after removing the filter membrane on it in deionized water.

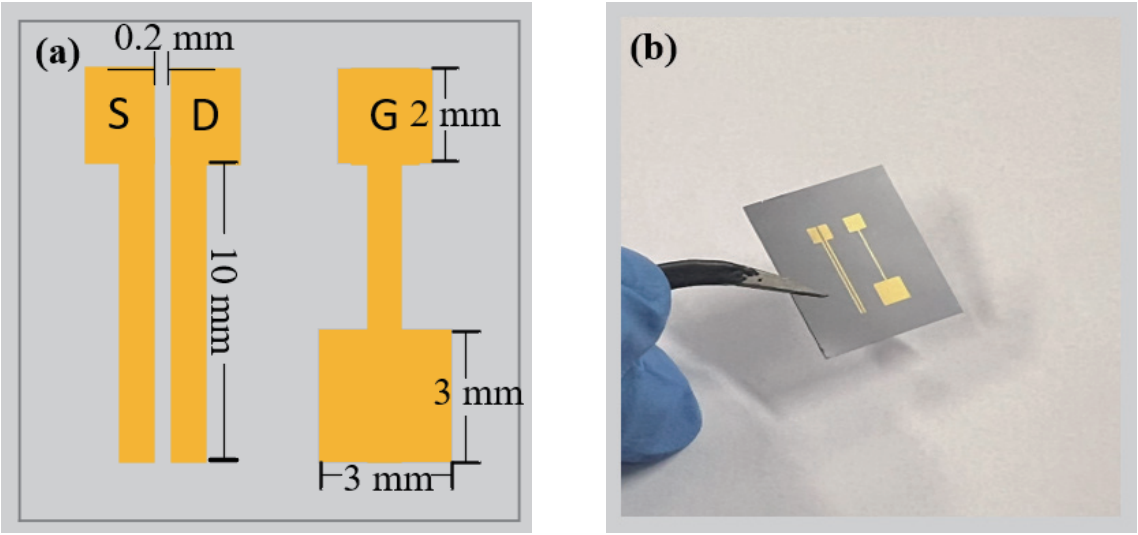

Fig. 2. (Color online) Planar transistor: (a) schematic diagram of electrode dimensions; (b) photograph of the device.

The graphene was air-dried at room temperature for approximately 20 min, then placed in an oven and dried at a low temperature of about 60 °C for 30 min. After cooling to room temperature, the device was cleaned twice with acetone. The graphene was then immersed in acetone and heated at 70 °C for 3 h to remove the surface PMMA layer. Finally, the device was cleaned twice with deionized water and annealed at 200 °C for 1 h to obtain the blank device [Fig. 2(b)].

2.2.3 Gate modification of carbon quantum dots

Carbon quantum dots were chosen to be modified on the larger-area gold gate surface, with mercaptoacetic acid ($HS{-}CH_2{-}COOH$) selected as the molecular bridge to achieve stable bonding. Figure 3 illustrates the process of modifying boronic acid carbon quantum dots on the gate electrode. First, 10 μL of 50 mM methacrylic acid (MAA) was dropped onto the gate electrode and left to react overnight in the dark to modify the carboxyl groups. After washing the device with deionized water, a mixture of 10 μL of 0.2 mM EDC and 0.5 mM NHS was dropped onto the gate to activate the carboxyl groups for 2 h. The device was then washed again with deionized water, followed by the addition of 10 μL of 0.5 mg/mL carbon quantum dot aqueous solution that was allowed to react with the gate for 3 h. Finally, the device was cleaned with deionized water to remove any unbound carbon quantum dots and residual materials.

2.3 Testing principles and methods

2.3.1 Double-layer capacitance effect

The liquid-gated graphene field-effect transistor is a type of electrolyte-gate controlled field-effect transistor. Figure 4 illustrates the redistribution of cations (blue) and anions (red) in the liquid electrolyte under an applied voltage, forming double electric layers at the gate/electrolyte and electrolyte/graphene interfaces, respectively. As shown in Fig. 4(a), under a negative gate

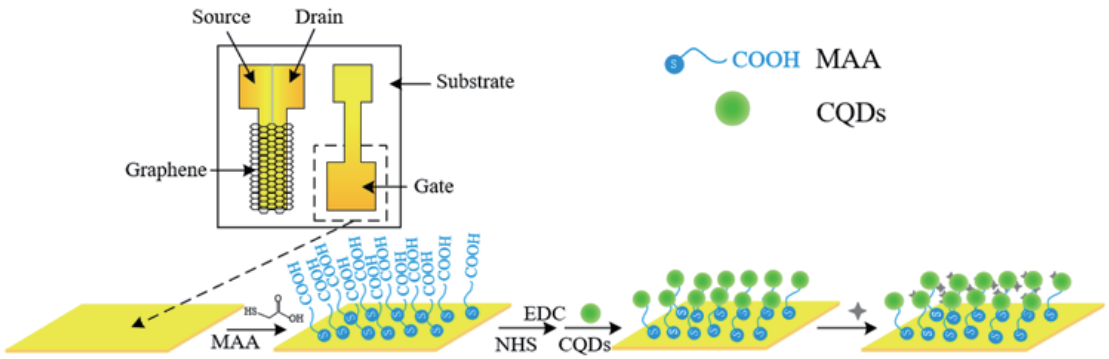

Fig. 3. (Color online) Schematic illustration of the process of fabricating carbon quantum dot–functionalized liquid-gated graphene field-effect transistor.

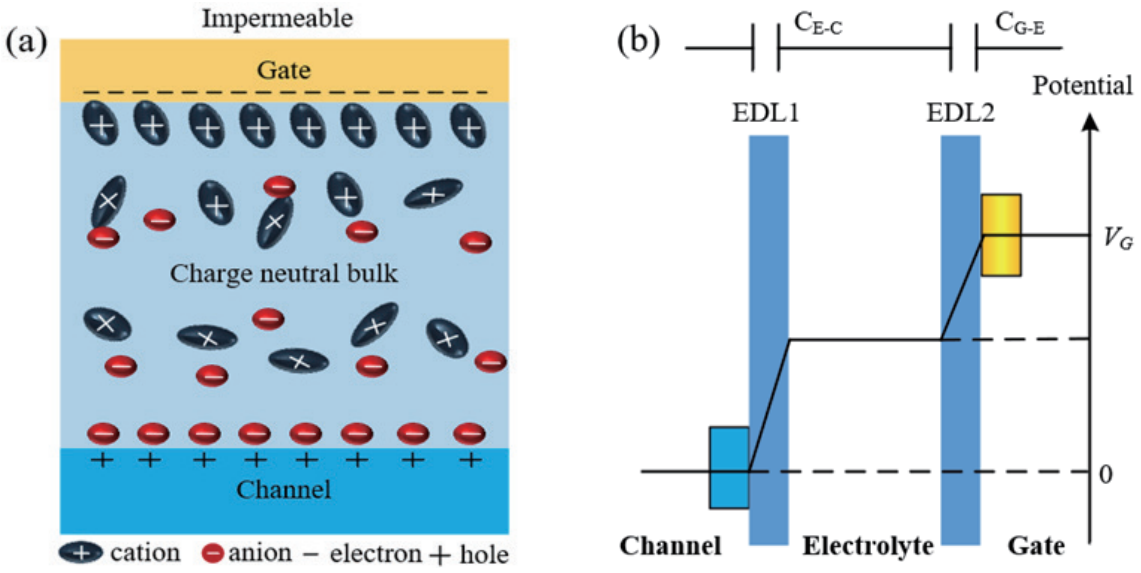

(a) (b)

Fig. 4. (Color online) Electrolyte-gated electrostatic coupling: (a) double-layer formation; (b) equivalent capacitance division.

bias, cations migrate to the gate/electrolyte interface, while anions move to the electrolyte/channel interface, forming double electric layers at their respective interfaces. While under a positive gate bias, the movement of positive and negative ions will be opposite. Thus, the capacitance of the sensor can be equivalent to two double-layer capacitors connected in series [Fig. 4(b)]. Typically, the capacitance at the electrolyte/channel interface is small, so this capacitance determines the total capacitance value.

It can be seen that, under a negative gate bias, anions in the electrolyte accumulate at the electrolyte/channel interface, inducing an equal number of holes in the p-type channel. Under the effect of source-drain voltage, these holes move within the channel, generating source–drain current [Fig. 4(a)]. During this process, the holes in the channel are completely generated through electrostatic coupling via the double-layer capacitors. In the experiment, electrons and holes in the graphene channel respond to such charge distribution, thereby adjusting the carrier concentration in the channel and becoming the physical basis for the liquid-gate modulation of electrostatic coupling field-effect transistors.

Furthermore, as shown in Fig. 4(b), for an electrolyte-gate–controlled field-effect transistor, the applied V_G is distributed across the gate/electrolyte and electrolyte/channel interfaces. This can be expressed by

$$V_G = V_{E\text{-}C} + V_{G\text{-}E} = \left(1 + \frac{C_{E\text{-}C}}{C_{G\text{-}E}}\right) V_{E\text{-}C} = (1+\gamma) V_{E\text{-}C}. \tag{1}$$

In the formula, $V_{G\text{-}E}$ and $V_{E\text{-}C}$ represent the voltages applied across the gate/electrolyte and electrolyte/channel interfaces, respectively. γ is the ratio of the capacitance at the electrolyte/channel interface ($C_{E\text{-}C}$) to that at the gate/electrolyte interface ($C_{G\text{-}E}$).

2.3.2 Dirac current–voltage (*I–V*) bipolar transfer characteristic testing

As shown in Fig. 5, the source, drain, and gate of the graphene transistor are connected to a digital source meter, with the source grounded. A voltage of 0.1 V (denoted as V_D) is applied between the drain and the source, and a voltage range of 0–1 V (denoted as V_G) is applied between the gate and the source. Phosphate-buffered saline is used as the electrolyte for measurement, and the TonghuiExpert software is utilized to set a scan rate of 0.02 V/s. Then, the Dirac current–voltage bipolar transport characteristics of the device are tested, and the transfer characteristic curve is plotted with the gate–source voltage V_G on the horizontal axis and the drain current I_D on the vertical axis.

Accordingly, the Dirac point voltage V_{Dirac} for each transfer characteristic curve was determined as the gate–source voltage V_G corresponding to the minimum point of the drain current I_D in the measured I_D–V_G curve. This minimum point was identified mathematically by fitting the data around the current nadir with a polynomial function and locating its vertex, ensuring the precise and reproducible extraction of V_{Dirac} for the subsequent analysis of concentration-dependent shifts.

2.3.3 Channel current testing

As shown in the schematic diagram of the testing setup in Fig. 5, the source, drain, and gate of the graphene transistor are equally connected to the digital source meter, with the source grounded. Fixed voltages are respectively applied to both the drain–source electrodes and gate–source electrodes, with the drain voltage V_D set to 0.1 V and the gate voltage V_G set to 0.55 V. Then, the variation in channel current in environments containing different concentrations of glucose, sucrose, starch, and sialic acid is monitored in real time, and the time–current response curve is plotted with the time on the horizontal axis and the drain or channel current I_D on the vertical axis.

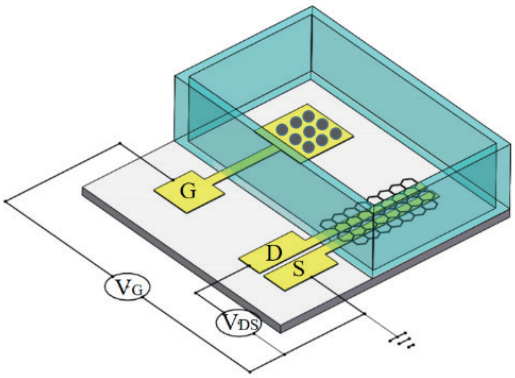

Fig. 5. (Color online) Schematic diagram of the testing setup for carbon quantum dot–functionalized liquid-gated graphene field-effect transistor.

Specifically, all electrical measurements, including the bipolar transfer characteristic testing and channel current testing, were performed in a low-ionic-strength PBS working solution. This solution was prepared by diluting the aforementioned PBS concentrate with ultrapure water at a volume ratio of 1:100. This resulting solution is referred to as 0.1 × PBS throughout this work. The use of a low-ionic-strength buffer extends the Debye screening length, which is essential for achieving high field-effect sensitivity and the ultralow detection limits reported herein.

3. Results and Discussion

3.1 Characterization of carbon quantum dots

Figure 6(a) shows the TEM image of the phenylboronic acid carbon quantum dots, and Fig. 6(b) shows the corresponding fluorescence characteristics. From Fig. 6(a), it can be observed that the phenylboronic acid carbon quantum dots are spherical and exhibit a particle size of less than 10 nm and a uniform distribution without notable aggregation. Furthermore, from the fluorescence characteristics in Fig. 6(b), it is evident that the synthesized carbon quantum dots exhibit green fluorescence, indicating that the maximum emission wavelength is 506 nm at an excitation wavelength of 375 nm, which also demonstrates the successful synthesis of the carbon quantum dots.

3.2 Detection of glucose molecules

3.2.1 Dirac *I*–*V* bipolar transfer characteristics

Figure 7(a) shows the transfer characteristic curve of the carbon quantum dot–functionalized liquid-gated graphene transistor in response to different concentrations of glucose solutions. Firstly, the transfer characteristic curve of the device exhibits a typical bipolar behavior, with the existence of the lowest Dirac point voltage. In accordance with the principle diagram of the

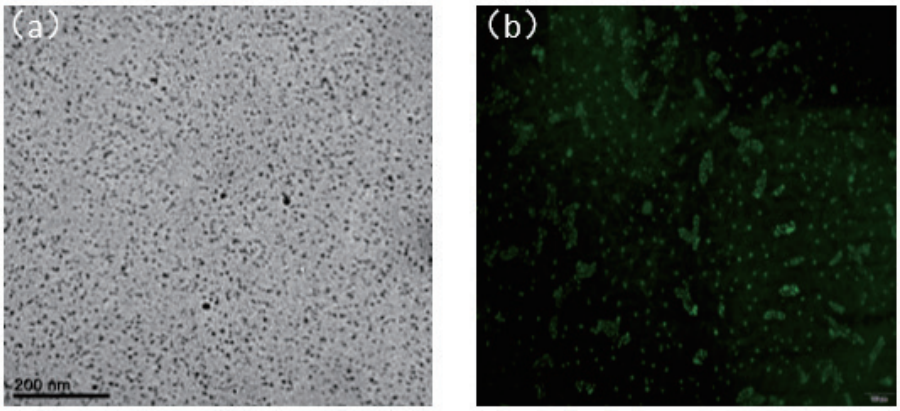

Fig. 6. (Color online) Phenylboronic acid carbon quantum dots: (a) TEM image; (b) fluorescence spectrum.

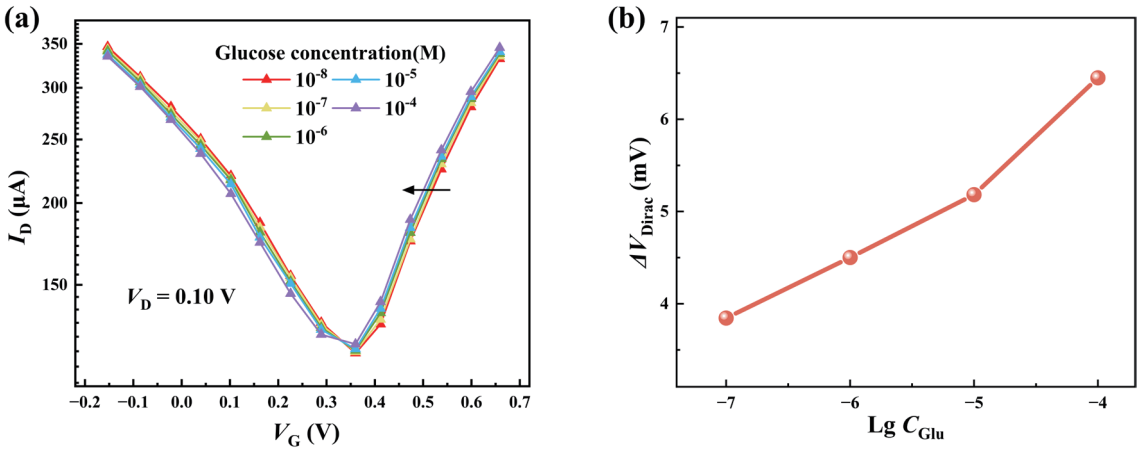

Fig. 7. (Color online) Response of carbon quantum dot–functionalized liquid-gated graphene field-effect transistor to different glucose concentrations: (a) transfer characteristics; (b) Dirac point voltage shift.

electrostatic coupling field effect shown in Fig. 4, with the Dirac point as the center, when the gate voltage is lower than the Dirac point voltage, the device exhibits hole conduction (p-type), and when the gate voltage is higher than the Dirac point voltage, the device exhibits electron conduction (n-type), which fully reflects the unique electronic properties of graphene. Additionally, a positive Dirac point voltage indicates that the graphene channel is p-type-doped, which is caused by factors such as water or oxygen molecule adsorption from the environment, substrate charges, and transferred residues.

Furthermore, in Fig. 7(a), it can be seen that as the glucose concentration gradually increases, the transfer characteristic curve of the device shifts horizontally to the left, towards more negative gate voltages, and the shift of Dirac point voltage shows an approximately linear relationship with the glucose concentration [Fig. 7(b)]. This phenomenon indicates that the phenylboronic acid carbon quantum dots modified on the gate surface can form reversible boronic ester bonds with the cis-diol groups in glucose molecules. As shown in Fig. 8(a), when glucose is added, the boronic groups on the surface of the carbon quantum dots react with glucose, where two boronic groups bond with one glucose molecule. The oxidation state of boron atoms increases from +3 to +4, losing two electrons ($2e^-$) and forming Faradaic current. The electrons transfer to the gate electrode, changing the potential distribution of the device and causing a change in double-layer voltage drop [Fig. 8(b)]. The increased voltage drop at the electrolyte/channel interface means that a smaller gate voltage is needed to obtain the same channel current, which results in a notable leftward shift of the bipolar characteristic curve. Additionally, during this reaction process, some protons (H^+) from the hydroxyl groups will dissociate, leaving a negatively charged oxygen ion (O^-), which reduces the distance of the gate/electrolyte double layer and increases the capacitance. This leads to a decrease in the ratio γ of the electrolyte/channel capacitance to the gate/electrolyte capacitance, which corresponds to the redistribution of the voltage drop across the two double layers. At the same time, the negatively charged oxygen ion (O^-) facilitates the electron transfer at the interface, causing a change in local

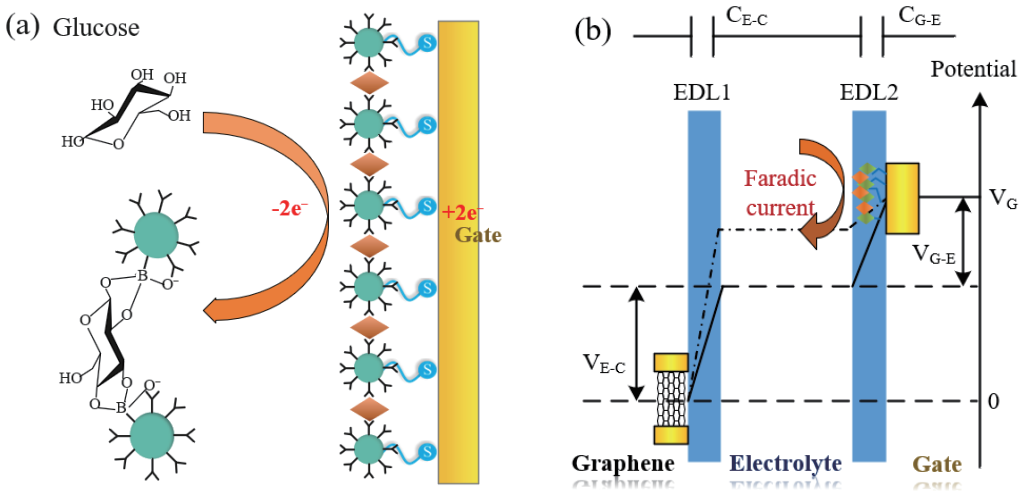

Fig. 8. (Color online) Formation of cyclic boronate ester between phenylboronic acid carbon quantum dots and glucose molecules: (a) schematic illustration of redox reaction accompanied by electron transfer; (b) schematic illustration of double-layer potential drop variation.

charge distribution and altering the carrier concentration in the graphene channel, thereby significantly shifting the transfer curve to the left.

Thus, it can be observed that after glucose is added, electrons are transferred to the gate, which lowers the gate/electrolyte voltage drop and increases the electrolyte/channel voltage drop. As a result, the voltage drop across the two double layers is redistributed. Because of the intrinsic amplification characteristics of the transistor, the Dirac point of its transfer characteristic curve will shift owing to the change in gate interface potential. This behavior indicates that the device can sensitively capture the electrical response caused by changes in glucose concentration and can demonstrate the ability to quantitatively detect analytes containing cis-diol structures as well as the stable concentration dependence, providing a basis for the subsequent analysis of sensitivity and detection limits.

3.2.2 Current response characteristics

Under the condition of the electrolyte-gate–controlled field effect, the channel current detection and its sensitivity to the electrolyte/channel interface voltage offer a more intuitive, real-time monitoring capability and broader application prospects than traditional voltage detection. Figure 9 shows the time response of the channel current and the corresponding relationship between channel current changes and glucose concentration under a drain voltage of 0.1 V and a gate voltage of 0.55 V, as glucose of different concentrations is added to a buffered saline electrolyte. In Fig. 9(a), it can be observed that the channel current of the device exhibits good time response to the addition of different concentrations of glucose solutions, with the channel current gradually increasing with the glucose concentration. This indicates that the device exhibits a more pronounced current response at higher glucose concentrations. Research has shown that the device can detect glucose concentrations with a detection limit as low as 10

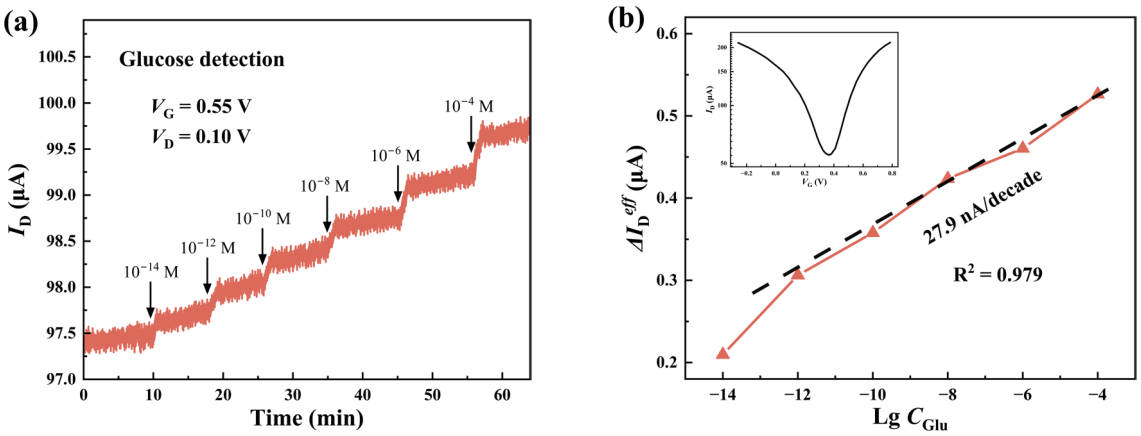

Fig. 9. (Color online) Response of carbon quantum dot–functionalized liquid-gated graphene field-effect transistor to different glucose concentrations: (a) time-dependent variation in channel current; (b) correlation between channel current change and logarithm of glucose concentration (inset: transfer characteristics of the device during detection).

Table 1
Glucose detection results.

Detection method	Detection material	Lowest detection	Detection range	Reference
Electrochemical method	Metal-organic framework/Nickel foam	1.3 nM	1 μM–3 mM	(19)
Electrochemical transistor	Chitosan/graphene/ glucose oxidase	10 nM	10 nM–1 μM	(20)
Electrochemical method	Cu_3N nanowires/ copper foam	10 nM	0.1–10 nM	(21)
Electrochemical method	$Ni(OH)_{2/3}D$ graphene	24 nM	24 nM–1.2 mM	(22)
Electrochemical method	Metal-organic framework/carbon nanotubes	0.6 μM	1 μM–0.3 mM	(23)
Electrochemical transistor method	Carbon–copper composite catalytic material	1 nM	1 nM–3.5 μM	(24)
Liquid-gated graphene transistor	Phenylboronic acid carbon quantum dots	10 fM	1 pM–0.1 mM	This work

fM [Fig. 9(a)], which is several orders of magnitude lower than the limits of other reported methods (as shown in Table 1), demonstrating the excellent sensitivity and response characteristics of the sensor in glucose detection. Furthermore, the relationship between current variation and the logarithm of glucose concentration displayed in Fig. 9(b) shows that the current change has good linear relationship with the logarithmic value of glucose concentration within the range of 10 fM to 0.1 mM. The calculated slope is 27.9 nA/decade, with an R^2 value of 0.979, indicating a high degree of linearity.

3.3 Detection of sucrose and starch molecules

3.3.1 Bipolar transfer characteristics of sucrose

Figure 10 shows the transfer characteristic curves of the carbon quantum dot–functionalized liquid-gated graphene transistor in response to different concentrations of sucrose solutions. From the figure, it can be seen that the transfer characteristic curves still exhibit typical bipolar behavior, but as the sucrose concentration increases, there is no significant overall leftward shift in the transfer curves. This is because sucrose is a disaccharide formed by the α-1, β-2-glycosidic bond between C1 of glucose and C2 of fructose. It does not contain any adjacent free hydroxyl groups, meaning that sucrose molecules lack the cis-diol structures that can interact with the boronic acid groups on the carbon quantum dots [Fig. 1(b)].

3.3.2 Bipolar transfer characteristics of starch

As shown in Fig. 11, the carbon quantum dot–functionalized liquid-gated graphene transistor exhibits a low direct detection capability for starch, with little notable change in channel current or the transfer characteristic curve. This is because starch, as a polymeric polysaccharide, contains cis-diol structures, but most of these cis-diol structures are obscured by glycosidic bonds and steric hindrance, limiting the available sites in the starch structure that can interact with the boronic acid groups. As a result, the device shows a weak response to starch structures. This result stands in stark contrast to the pronounced leftward shift in response to cis-diol molecules such as glucose, proving that the device's recognition is not only dependent on the "boronic acid-diol" specific chemical interaction sites but also affected by factors such as glycosidic bonds and steric hindrance, making it difficult for some polymeric polysaccharides to effectively bind with the boronic acid groups. Thus, the device maintains good baseline stability

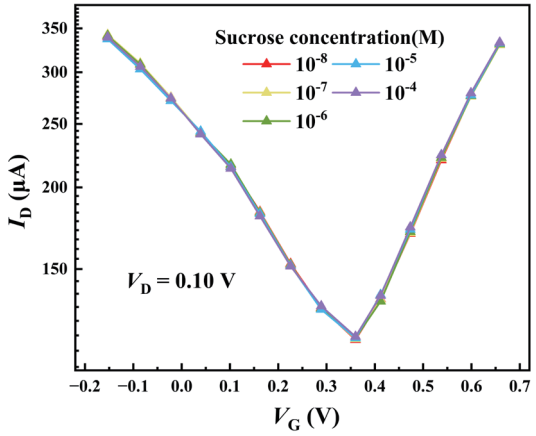

Fig. 10. (Color online) Transfer characteristics of carbon quantum dot–functionalized liquid-gated graphene field-effect transistor in response to different sucrose concentrations.

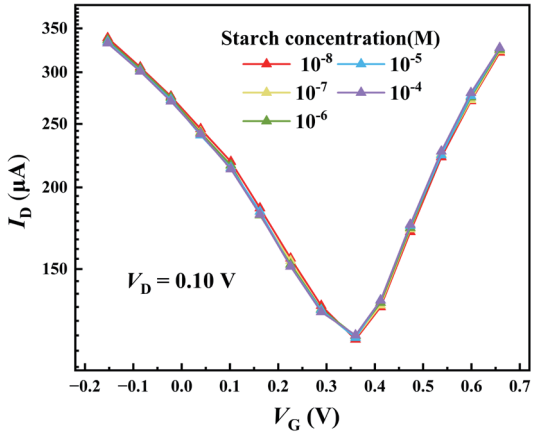

Fig. 11. (Color online) Transfer characteristics of carbon quantum dot–functionalized liquid-gated graphene field-effect transistor in response to different starch concentrations.

and interference resistance under nonspecific large-molecule backgrounds, which is beneficial for achieving high specificity and low false positives in the detection of cis-diol molecules in complex biological media, highlighting the selective advantages and application potential of this sensing platform.

3.4 Detection of sialic acid molecules

3.4.1 Dirac *I*–*V* bipolar transfer characteristics

Figure 12(a) shows the transfer characteristic curves of the liquid-gated graphene transistor in response to different concentrations of sialic acid solutions. As seen in Fig. 12, with the increasing concentration of sialic acid, the transfer characteristic curve shifts notably to the left. This shift is attributed to the interaction between the cis-diol structure in the sialic acid molecules and the boronic acid groups on the phenylboronic acid carbon quantum dots, which undergoes a redox reaction, causing changes in double-layer voltage drop and channel current. Similarly, the shift in Dirac point voltage as a function of sialic acid concentration shows an approximately linear relationship [Fig. 12(b)]. Note that, compared with glucose, the shift in Dirac point voltage is slightly smaller. This is because sialic acid molecules have a nine-carbon backbone, and their spatial structure affects the effective exposure of the cis-diol group. The stable boronic ester formation at the "neighboring cis-diol" sites is mainly located at the terminal glycerol side chain, and the carboxyl end (COO^-) of sialic acid can also affect its behavior on charged surfaces or under different pH conditions, leading to a slight reduction in binding efficiency. However, overall, the device still exhibits sensitive detection capability for sialic acid and maintains stable response characteristics under differet in molecular spatial structures.

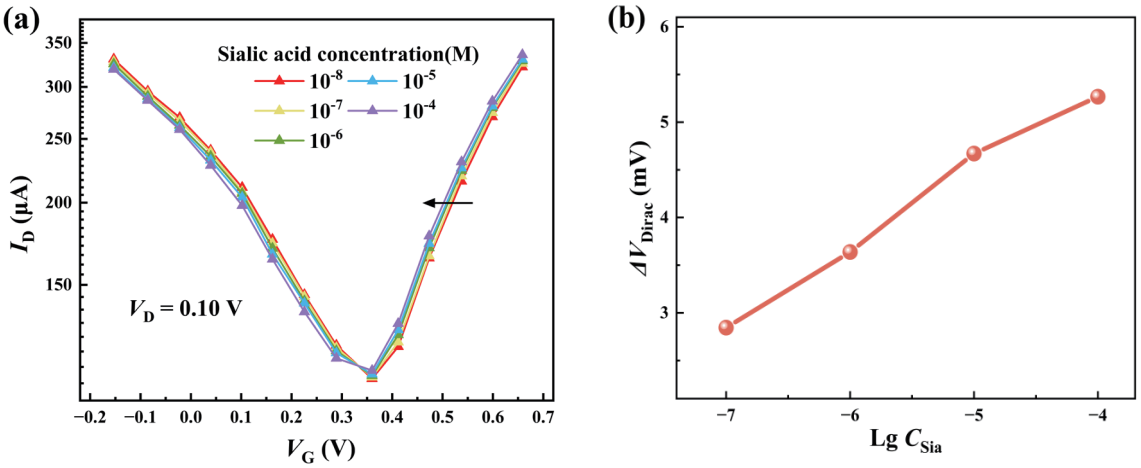

Fig. 12. (Color online) Response of carbon quantum dot–functionalized liquid-gated graphene field-effect transistor to different sialic acid concentrations: (a) transfer characteristics; (b) Dirac point voltage shift.

3.4.2 Current response characteristics

Figure 13 shows the time response of the channel current and the relationship between different concentrations of sialic acid and the channel current changes when different concentrations of sialic acid are added to the buffered saline electrolyte, with a drain voltage of 0.1 V and a gate voltage of 0.55 V. In Fig. 13(a), it can be observed that under fixed voltage conditions, as the concentration of sialic acid increases, the channel current gradually increases, and the minimum detection limit can also reach 10 fM, demonstrating good current response. Figure 13(b) further shows the logarithmic relationship between channel current variation and sialic acid concentration. It also indicates that within the range of 10 fM to 0.1 mM, the current change has good linear relationship with the sialic acid concentration, with a linear slope of 29.1 nA/decade. This means that the device's sensitivity to sialic acid detection is higher than that for glucose molecules, with a fitting coefficient $R^2 = 0.981$, ensuring the validity of the test. It can be seen that, compared with glucose detection, although the absolute current response for sialic acid is slightly lower than that for glucose, its current change amplitude (ΔI) is larger. This again indicates that the cis-diol groups in sialic acid molecules can induce stronger interface charge disturbances during the binding process, thereby amplifying the electrical response. Therefore, the device not only enables the highly sensitive detection of sialic acid but also shows superior response characteristics in terms of the signal change amplitude compared with glucose, highlighting its potential advantages in detecting complex biomolecules.

3.5 Comprehensive performance evaluation of the sensor

3.5.1 Interference immunity and selectivity testing

Building upon the demonstrated excellent detection capability for glucose and sialic acid, the selectivity of the phenylboronic acid carbon quantum dot–functionalized liquid-gated graphene

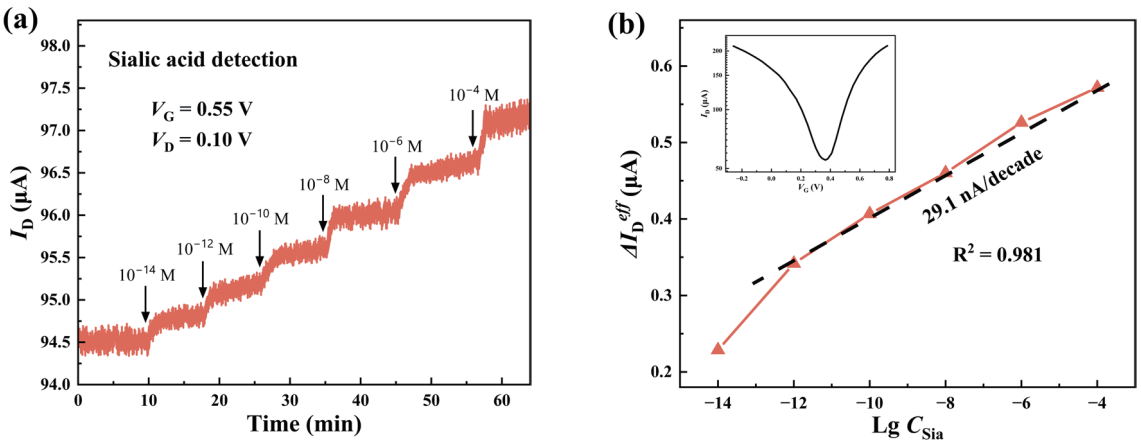

Fig. 13. (Color online) Response of carbon quantum dot–functionalized liquid-gated graphene field-effect transistor to different sialic acid concentrations: (a) time-dependent variation in channel current; (b) correlation between channel current change and logarithm of sialic acid concentration (inset: transfer characteristics of the device during detection).

transistor sensor was further evaluated against common serum interferents, including ascorbic acid, Na^+ (from NaCl), and K^+ (from KCl). As shown in Fig. 14, at an identical concentration of 0.1 mM, the sensor's current response to all tested interferents was significantly lower than its response to the target analytes, glucose and sialic acid. This differential selectivity originates from distinct mechanisms for each interferent: sucrose lacks the cis-diol moiety necessary for recognition (as discussed earlier in Sect. 3.3.1); starch, although containing cis-diol groups, is inaccessible owing to steric hindrance (as discussed earlier in Sect. 3.3.2); Na^+ and K^+ ions are electrostatically screened via Debye shielding, preventing effective field-effect modulation; and ascorbic acid, despite possessing cis-diol groups, is rapidly oxidized and deactivated under the detection conditions (pH 7.4). Collectively, these results confirm that the sensor produces only negligible responses to common biological interferents, exhibiting exceptional anti-interference ability and high selectivity. This performance establishes a solid foundation for its potential application in complex biological milieus.

3.5.2 Repeatability and temporal stability testing

To assess the practical reliability of the sensor, its reproducibility across different batches and temporal stability were systematically evaluated. First, three phenylboronic acid carbon quantum dot–functionalized liquid-gated graphene transistor sensors fabricated in separate batches were used to detect 0.1 mM glucose solution under identical testing conditions, and their current responses were recorded. The results demonstrated that the three devices exhibited highly consistent response signals, with a relative standard deviation of only 3.9%, indicating excellent repeatability and process consistency in batch fabrication. Subsequently, the temporal stability of the sensor was investigated by performing transfer characteristic measurements on the same device after 1, 3, 5, and 7 days of storage. As shown in Fig. 15, the transfer characteristic curves obtained at different time points overlapped closely, confirming negligible performance degradation over time. These findings collectively demonstrate that the sensor maintains reliable electrical performance during repeated use and short-term storage, underscoring its robustness and suitability for real-world applications.

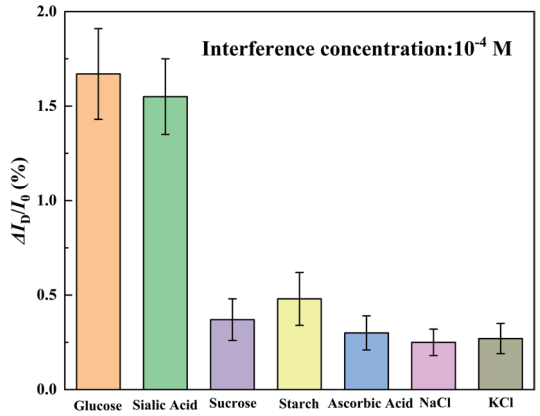

Fig. 14. (Color online) Statistical chart of current response ratio of carbon quantum dot–functionalized liquid-gated graphene transistor to various interferents.

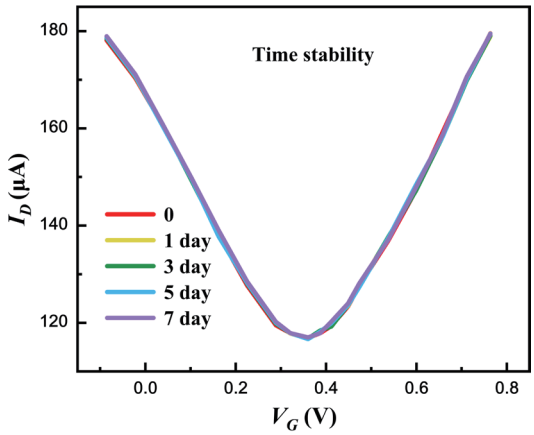

Fig. 15. (Color online) Temporal stability evaluation of the carbon quantum dot–functionalized liquid-gated graphene field-effect transistor.

In additon, note that the current proof-of-concept demonstrations were performed in a low-ionic-strength buffer to enhance signal response. Future work will focus on optimizing the sensor interface to enable its reliable operation in physiologically relevant media, which is a crucial step toward practical clinical applications.

4. Conclusions

In this study, a phenylboronic acid carbon quantum dot–functionalized liquid-gated graphene transistor sensor was successfully developed, achieving high sensitivity and specificity in recognizing sugar molecules containing cis-diol structures. By introducing boronic acid groups onto the surface of the carbon quantum dots and fixing them onto the gate electrode, the device successfully enabled the electrical detection of target molecules containing cis-diol structures with a minimum detection limit of 10 fM, which is several orders of magnitude lower than the limits in previous reports. Moreover, the device demonstrated excellent linear response within the concentration range of 10 fM to 0.1 mM, reflecting a wide linear range and reliable quantitative performance. Owing to the molecular-level selective recognition, the device showed low or zero cross-reactivity with such interfering substances as sucrose and starch that lack or have difficult-to-expose neighboring diol sites, and the common serum interferents, such as ascorbic acid, Na^+, and K^+. This ability to maintain stability and resistance to interference in complex biological matrices highlights the dual advantages of selectivity and stability. Additionally, the device features fast response, miniaturization potential, and ease of integration, showcasing its potential for the specific recognition of sugar molecules as well as offering a new electrical detection approach for tumor biomarker detection and the early diagnosis of related diseases.

References

1 R. Shandilya, A. Bhargava, N. Bunkar, R. Tiwari, I. Y. Goryacheva, and P. K. Mishra: Biosens. Bioelectron. **130** (2019) 147. https://doi.org/10.1016/j.bios.2019.01.034
2 R. V. Devi, M. Doble, and R. S. Verma: Biosens. Bioelectron. **68** (2015) 688. https://doi.org/10.1016/j.bios.2015.01.066
3 U. Laraib, S. Sargazi, A. Rahdar, M. Khatami, and S. Pandey: Int. J. Biol. Macromol. **195** (2022) 356. https://doi.org/10.1016/j.ijbiomac.2021.12.052
4 A. Varki: Trends Mol. Med. **14** (2008) 351. https://doi.org/10.1016/j.molmed.2008.06.002
5 W. Zhu, Y. Zhou, L. Guo, X. Xu, Y. Wang, and F. Xue: Cell Death Discov. **10** (2024) 415. https://doi.org/10.1038/s41420-024-02180-3
6 A. L. Galant, R. C. Kaufman, and J. D. Wilson: Food Chem. **188** (2015) 149. https://doi.org/10.1016/j.foodchem.2015.04.071
7 S. Shilo, A. Keshet, H. Rossman, A. Godneva, Y. Talmor-Barkan, Y. Aviv, and E. Segal: Nat. Med. **30** (2024) 1424. https://doi.org/10.1038/s41591-024-02908-9
8 R. Zhang and Y. Jia: ACS Sens. **6** (2021) 3024. https://doi.org/10.1021/acssensors.1c00949
9 R. F. de Oliveira, P. A. Livio, V. Montes-García, S. Ippolito, M. Eredia, P. Fanjul-Bolado, M. B. González García, S. Casalini, and P. Samorì: Adv. Funct. Mater. **29** (2019) 1905375. https://doi.org/10.1002/adfm.201905375
10 S. Jarić, A. Kudriavtseva, N. Nekrasov, A. V. Orlov, I. A. Komarov, L. A. Barsukov, I. Gadjanski, P. I. Nikitin, and I. Bobrinetskiy: Microchem. J. **196** (2024) 109611. https://doi.org/10.1016/j.microc.2023.109611
11 N. Gao, R. Zhou, B. Tu, T. Tao, Y. Song, Z. Cai, H. He, G. Chang, Y. Wu, and Y. He: Anal. Chim. Acta **1239** (2023) 340719. https://doi.org/10.1016/j.aca.2022.340719
12 C. Kou, X. Xu, Y. Bao, Z. Guo, and L. Niu: Chemosensors **13** (2025) 56. https://doi.org/10.3390/chemosensors13020056
13 R. F. de Oliveira, V. Montes-García, P. A. Livio, M. B. González-García, P. Fanjul-Bolado, S. Casalini, and P. Samorì: Small **18** (2022) 2201861. https://doi.org/10.1002/smll.202201861
14 S. Sarkar, S. Hazra, S. Patra, and M. Gogoi: TrAC, Trends Anal. Chem. **117978** (2024) 1. https://doi.org/10.1016/j.trac.2024.117978
15 C. Zhang, P. Miao, M. Sun, M. Yan, and H. Liu: Small **15** (2019) 1901867. https://doi.org/10.1002/smll.201901867
16 B. Patrick, T. Akhtar, R. Kousar, C.-C. Huang, and X.-G. Li: Int. J. Mol. Sci. **24** (2023) 6600. https://doi.org/10.3390/ijms24076600
17 W. Zhu, Y. Zhou, L. Guo, and S. Feng: Cell Death Discov. **10** (2024) 415. https://doi.org/10.1038/s41420-024-02180-3
18 J. Cheeseman, G. Kuhnle, D. I. R. Spencer, and H. M. I. Osborn: Bioorg. Med. Chem. **36** (2021) 115882. https://doi.org/10.1016/j.bmc.2020.115882
19 Y. Li, M. Xie, X. Zhang, Q. Liu, D. Lin, C. Xu, F. Xie, and X. Sun: Sens. Actuators, B **278** (2019) 126. https://doi.org/10.1016/j.snb.2018.09.076
20 C. Liao, M. Zhang, L. Niu, Z. Zheng, and F. Yan: J. Mater. Chem. B **2** (2014) 191. https://doi.org/10.1039/c3tb20451k
21 Z. Wang, X. Cao, D. Liu, S. Hao, R. Kong, G. Du, A. M. Asiri, and X. Sun: Chemistry **23** (2017) 3911. https://doi.org/10.1002/chem.201700366
22 I. Shackery, U. Patil, M.-J. Song, J. S. Sohn, S. Kulkarni, S. Some, S. C. Lee, M. S. Nam, W. Lee, and S. C. Jun: Electroanalysis **27** (2015) 2209. https://doi.org/10.1002/elan.201500009
23 X. Zhang, J. Luo, P. Tang, J. R. Morante, J. Arbiol, C. Xu, Q. Li, and J. Fransaer: Sens. Actuators, B **253** (2017) 1126. https://doi.org/10.1016/j.snb.2017.07.024
24 T. Tao, S. Ye, M. Ma, N. Gao, Z. Cai, X. Liu, G. Chang, and Y. He: Chin. J. Anal. Chem. **49** (2021) 387. https://doi.org/10.19756/j.issn.0253-3820.201594

About the Authors

Jiahui Li received his B.S. degree in automation from Liaoning Institute of Science and Technology in 2023. He is currently pursuing his M.S. degree in instrument science and technology with North China University of Science and Technology, expected to be completed in 2026. His research interests include the design and fabrication of micro/nanosensors, the development of detection systems, and biosensing techniques based on graphene transistors for medical applications. (3141560252@qq.com)

Qin Wei graduated from Tianjin University Ren'ai College with a Bachelor of Engineering degree in Automation in 2024. He is currently pursuing a M.S. degree in instrument science and technology at North China University of Science and Technology, expected to be completed in 2027. (2572690691@qq.com)

Chunrui Chang received her M.S. degree in theoretical physics from Hebei University of Technology in 2008 and her Ph.D. degree in material physics and chemistry from the Suzhou Institute of Nano-Tech and Nano-Bionics, Chinese Academy of Sciences in 2011. She is currently an associate professor and a master's supervisor with the College of Science, North China University of Science and Technology. Her current research focuses on carbon nanocomposites and their device applications. (changchunrui@ncst.edu.cn)